THE JOURNAL OF PHYSICAL CHEMISTRY C

Article

Cite This: J. Phys. Chem. C 2018, 122, 20186−20193

pubs.acs.org/JPCC

Drastic Improvement in Gas-Sensing Characteristics of Phosphorene Nanosheets under Vacancy Defects and Elemental Functionalization

T. Kaewmaraya,[†,‡] L. Ngamwongwan,[†] P. Moontragoon,[†,‡] A. Karton,[§] and T. Hussain*[,§,∥]

[†]Integrated Nanotechnology Research Center, Department of Physics, Khon Kaen University, Khon Kaen 40002, Thailand

[‡]Nanotec-KKU Center of Excellence on Advanced Nanomaterials for Energy Production and Storage, Khon Kaen 40002, Thailand

[§]School of Molecular Sciences, The University of Western Australia, Perth, Western Australia 6009, Australia

[∥]Centre for Theoretical and Computational Molecular Science, Australian Institute for Bioengineering and Nanotechnology, The University of Queensland, Brisbane, Queensland 4072, Australia

ABSTRACT: Efficient chemical gas detection is of great importance for various functionalities (such as leakage detection of hazardous and explosive gases in industrial safety systems). The recent discovery of 2D black phosphorene (BlackP) has created intensive interests toward nanosensors because of its maximized surface-to-volume ratio and exceptional carrier mobility that potentially deliver the superior performance than the conventional transition-metal oxides sensors. In this work, we have performed first-principles DFT calculations coupled with the statistical analysis to unravel the structural, electronic, and gas-sensing characteristics of pristine, defected, and metal-substituted BlackP toward toxic H_2S and SO_2 gas molecules. Our findings have revealed that pristine BlackP weakly interacts with both H_2S and SO_2 by van der Waals (vdW) forces characterized by the small binding energies. The analysis of electronic properties via the density of states (DOS) indicates that there is a negligible change in DOS after gas exposure, which confirms insensitive sensing. To intensify the binding energies, we have considered defects (mono-, di-, tri-, and quad-vacancy) and substitutional impurities (Ti, Si, Mn, and Fe) as the incentives. The presence of mono- and divacancies remains less energetically sensitive to both gas species because of the low adsorption energies. Meanwhile, tri- and quad-vacancies induce the dissociative adsorption, not suitable for the reversible adsorption−desorption cycles. Substitutional doping by Fe atoms is found to be a feasible approach to enhance the sensing resolution of SO_2 detection because of the remarkable adsorption energy incorporated with the substantial variation in DOS after gas exposure. This modification in electronic properties is facilitated by the charge transfer mechanism from Fe 3d to P 3p which can generate the measurable electrical signal detected by the external circuit of the sensor.

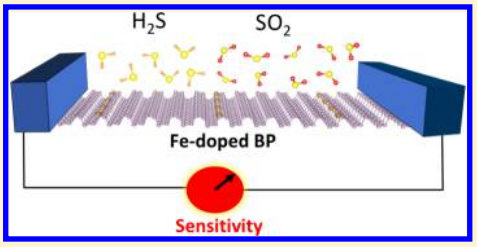

INTRODUCTION

Chemical gas detection has become one of the most crucial issues offering a wide range of applications, e.g., leakage detection of hazardous or explosive gases in industrial safety systems, air quality testing, and military monitoring.[1] A chemical gas sensor refers to a device that converts chemical reactions into analytically detectable signals. There are numerous kinds of gas detectors classified by the operational mechanism of the transducers, i.e., semiconductors, oxidation, and catalytic just to name a few. Among them, semiconducting oxides (such as TiO_2, ZnO, and SnO_2) are ubiquitous materials commercially available nowadays because of high sensitivity, low production costs, and device scalability. They detect the presence of target analytes by exploiting measurable changes in electrical conductivity, i.e., the local carrier concentration, before and after gas exposure. The change in conductivity is associated with the charge transfer mechanism between the gas molecules and the sensors where the former can act as either donors or acceptors. However, the resolution of semiconducting sensors is generally limited to 1 ppm (ppm).[1] This is due to the remarkable noise fluctuation fundamentally originated from thermal motion of charges and defects.[2] Hence, searching for sensing materials offering ultimate sensitivity in the order 1 part per billion (ppb) or even higher remains one of the key challenges in chemical sensing technology.

An innovative approach to attain ultrasensitivity is the use of emerging nanomaterials. This is because of the maximized surface-to-volume ratio as exemplified by the extraordinary resolution down to the order of ppb of carbon nanotubes and several kinds of semiconducting nanowires,[3,4] surpassing the resolution limit of existing semiconducting sensors. Additional interests have also expanded to atomically thin two-dimensional (2D) materials due to the key benefits such as rapid carrier mobility, unique planar morphology that enlarges the reactive gas-sensing area, superior mechanical stability, and room-temperature operation.[5−7] These unique features are preferential for practical chemical sensing applications. For instance, recent works have revealed that graphene[2] and MoS_2[8,9] sensing devices demonstrate exceptional performance

Received: July 16, 2018
Revised: August 11, 2018
Published: August 14, 2018

DOI: 10.1021/acs.jpcc.8b06803
J. Phys. Chem. C 2018, 122, 20186−20193

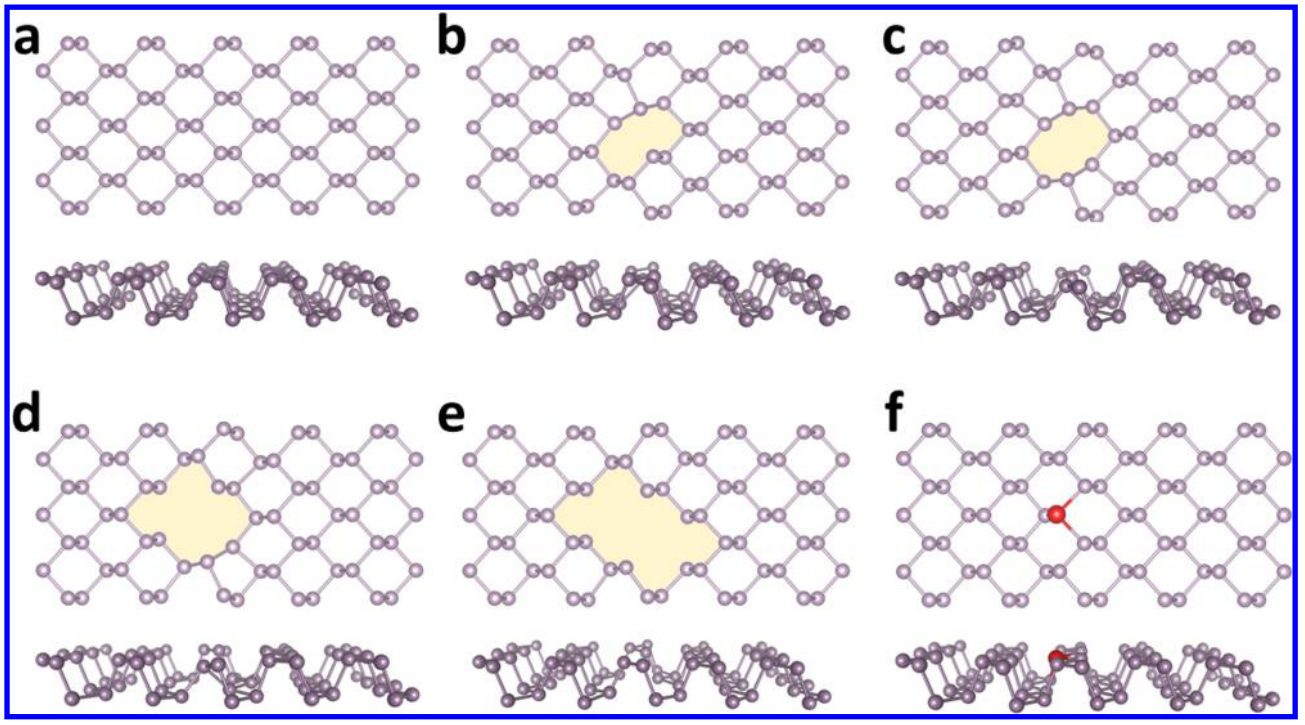

Figure 1. Crystal structures (bird's-eye and side views) of different kinds of phosphorene considered in this work: (a) pristine, (b) monovacancy (M-vac), (c) divacancy (D-vac), (d) trivacancy (T-vac), (e) quad-vacancy (Q-vac), and (f) Fe (Mn, Si, Ti)-doped. Light purple and red spheres represent P and Fe (Mn, Si, Ti) atoms.

toward various gas species. More recently, a 2D form of black phosphorus, named phosphorene (BlackP), was successfully fabricated.[10−12] This material shows many appealing properties. It possesses extraordinary carrier mobility (about 1000 $cm^2\ V^{-1}\ s^{-1}$ at room temperature),[10] which intriguingly exceeds that of other 2D semiconductors such as MoS_2 (approximately 200 $cm^2\ V^{-1}\ s^{-1}$).[13] Unlike graphene, BlackP is a direct-gap semiconductor of which the gap size depends on the number of layers.[14] Another feature is that electric and optical properties are anisotropic along the zigzag and the armchair directions due to its puckered wave-like structure with sp^3 bonding.[15] This puckered geometry results in the higher surface-to-volume ratio and lower out-of-plane electrical conductance than other 2D materials.[16,17] In particular, the latter gives rise to a more sensitive response to the target gas species near BlackP surface.[17] Furthermore, it also shows superior mechanical flexibility.[18] These mentioned features can practically facilitate the chemical sensing efficiency.

The gas-sensing functionality of BlackP for detecting selected important gases has been intensively reported.[5,17,19−21] The excellent sensitivity and selectivity of phosphorene for probing NO_2 at the concentration of 5 ppb in the dry environment has been experimentally confirmed.[17] However, it remains less sensitive to other important analytes, particularly sulfur-contained gas species (H_2S and SO_2).[22] This is due to weak van der Waals (vdW) interactions between gas molecules and the sensor, which are too weak to be detectable because no electrons are exchanged between gas molecules and phosphorene. The efficient detection of these toxic gases is of crucial importance. Colorless H_2S is a highly hazardous gas generally emitted from fuel cells, crude petroleum, volcanoes, and hot springs. Toxic SO_2 is available from manufacturing sulfuric acid and combustion of sulfur. Inhaling these gases at a concentration of more than 75 ppm (American Conference of Governmental Industrial Hygienists) is drastically harmful to the respiratory system.

A possible way to intensify adsorption energies from weak vdW to chemically strong interactions is either to dope impurity atoms or to create defects.[23−25] The explanation is ascribed to the fact that the introduction of suitable dopants yields more electron transfer between gas molecules and the 2D sensors. Therefore, the objectives of this work are to increase the gas-sensing sensitivity of phosphorene by means of introducing defects and impurities. The theoretical approach based on the so-called density functional theory (DFT), and a statistical model will be employed to attain useful information regarding adsorption energies and electronic properties of gas-adsorbed phosphorene.

■ COMPUTATIONAL AND MODELING DETAILS

Density functional theory (DFT) calculations were performed using VASP code.[26] The electron−ion interactions were treated by projector-augmented wave (PAW)[27] approach with the generalized-gradient approximation according to Perdew−Burke−Ernzerhof (PBE) formalism.[28] Free-standing phosphorene was modeled by 4 × 4 × 1 supercell consisting of 54 phosphorus atoms and the vacuum spacing of 20 Å was added along the *z*-direction to sufficiently decouple the interaction between periodic replicas. This supercell was based on an orthorhombic unit cell with the optimized lattice constants a = 3.314 Å and b = 4.376 Å. The k-point grids for Brillioun zone integration of 9 × 9 × 1 and 17 × 17 × 17 were used for structural optimizations and density of states (DOS) calculations, respectively. A cutoff energy of 500 eV for representing plane wave basis was used throughout the calculations because of being sufficient to attain reasonable energy convergence. The geometrical relaxations were

DOI: 10.1021/acs.jpcc.8b06803
J. Phys. Chem. C 2018, 122, 20186−20193

terminated when the Hellman−Feyman force exerting on each atom became less than 10^{-3} eV/Å.

The binding energies of the adsorbed gas molecules on phosphorene monolayer were determined by the following expression:

$$E_b = E_{BlackP+gas} - (E_{BlackP} + E_{gas}) \quad (1)$$

where gas = H_2S, SO_2.

In eq 1, the first, second, and third terms refer to the total energies of the phosphorene sheet adsorbed by the gas molecules, the corresponding bare phosphorene, and the independent gas molecule, respectively. Moreover, the formation energies of the vacancy defects were determined by the following formalism.

$$E_f = E_{(defected)} - \{(x - y)/x\}E_{pristine} \quad (2)$$

where E_f represents the formation energy, $E_{defected}$ denotes the total energy of defected phosphorene, $E_{pristine}$ is the total energies of pristine phosphorene, and x and y are the numbers of atoms in the phosphorene and of atoms removed, respectively. The calculated adsorption energies presented in this work have incorporated van der Waals interactions using Grimme approach.[29] In addition, the calculations of gas adsorption on to defected systems were spin-polarized to avoid the overestimation of adsorption energy because of the dipole moment-spin interaction.[21] The underlying charge transfer mechanism between the target gas molecule and phosphorene was investigated using Bader analysis.[30]

RESULTS AND DISCUSSION

We start with presenting the crystal structures of phosphorene considered in this work. The assembly of structurally relaxed geometries is given in Figure 1. The optimized pristine phosphorene (the bounding box) has the lattice constants a = 4.58 Å and b = 3.32 Å, P−P bond lengths of 2.22 and 2.26 Å, and P−P−P bond angles of 96.00 and 104.15°, consistent with the previous studies.[31] There are four kinds of neutral vacancies considered in this work, namely, monovacancy (M-vac), divacancy (D-vac), trivacancy (T-vacancy), and quad-vacancy (Q-vac). The presence of dangling bonds causes notable atomic rearrangements where the P atoms close to the vacant sites form new bonds with the nearby atoms. There is a drastic variation in the P−P distances, ranging from 2.20 to 2.50 Å as compared to those in the defect-free structure. This structural deformation leads to the reduction in the coordination number and the vacancy sites have consequently become chemically reactive to interacting with foreign gas molecules. In addition, the formation energies associated with M-vac, D-vac, T-vac, and Q-vac are −5.40, −4.46, −4.48, and −5.03 eV, respectively. Apparently, the formation of M-vac and T-vac are energetically more preferable than D-vac.[32] It is important to mention here that the formation energy of phosphorene, especially in case of M-vac, is much smaller than that of the most studied 2D system, graphene.[33]

The expected increase in chemical reactivity of BlackP with defects and impurities to gas molecules (here H_2S and SO_2) was exhaustively examined by searching for the lowest-energy structures. Numerous initial configurations of individual gas species were examined, and the corresponding adsorption energies after structural optimization were evaluated. In principle, the gas-sensing mechanism depends on the measurable change in the electrical conductivity of a sensor after exposing it to the target gas species. The adsorption of gas molecules can either increase or decrease the conductivity, depending on the variation in carrier concentration induced by the charge transfer between the target molecules and the sensor, i.e., the adsorbate acting as either a donor or an acceptor. The transfer is facilitated by the difference in the electronegativity. This fundamental mechanism coupled with chemical bonding is theoretically reflected by the adsorption energy. A strong adsorption energy represents a strong chemical bond where the charge transfer process takes place and it consequently induces the detectable contrast in the electrical resistivity. Hence, the contrast in conductivity therefore defines the sensitivity. In contrast, low adsorption energy indicates a weak vdW bond, which does not yield the marked change in resistivity. The appropriate adsorption energy should be around 1.00 eV, which represents weak chemical interaction and it also facilitates complete adsorption−desorption cycles with a reasonable recovery time by means of laser heating without the destruction of sensors' surface structures.[34−36]

The calculated adsorption energies corresponding to the most stable geometries are compiled in Figure 2. The

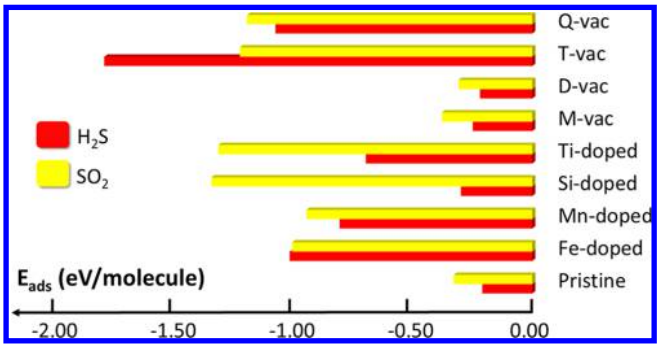

Figure 2. Adsorption energies of H_2S and SO_2 gas molecules adsorbed on to several kinds of phosphorene. The capital D defines dissociative adsorption.

computed adsorption energies indicate that pristine BlackP is less sensitive to both types of S-contained gases because of the low binding energies, 0.21 and 0.33 eV/molecule for H_2S and SO_2, respectively.[22] The H_2S molecule energetically adopts the vertical orientation where the H atoms direct toward the phosphorene surface (as shown in Figure 3). This binding configuration resembles that reported in the previous work.[22] The shortest H−P and S−P bond distances are 2.91 and 3.91 Å, and the H−S−H bond angle remains unaffected. Meanwhile, Figure 4 reveals that the SO_2 molecule prefers to be adsorbed on the hollow site with horizontal orientation pointing the S atom to bind to a phosphorus atom and a corresponding P−S bond distance of 3.00 Å. Like H_2S, the O−S−O bond angle is unaltered. Note that the adsorption energy of SO_2 is relatively higher than that of H_2S simply because the former directs S atom toward phosphorene and the difference in electronegativity between S and P is greater than that between H and P. In addition, it is worth mentioning that the H−S (S−O) bond distance in an isolated H_2S (SO_2) molecule is calculated to be 1.352 (1.455) Å. After adsorption onto pure BlackP, H−S (S−O) bond length becomes 1.351 (1.456) Å, resembling their original values. Apparently, the large bond lengths between the gas molecule and phosphorene and the negligible changes in the bond angles support the low binding

DOI: 10.1021/acs.jpcc.8b06803
J. Phys. Chem. C 2018, 122, 20186−20193

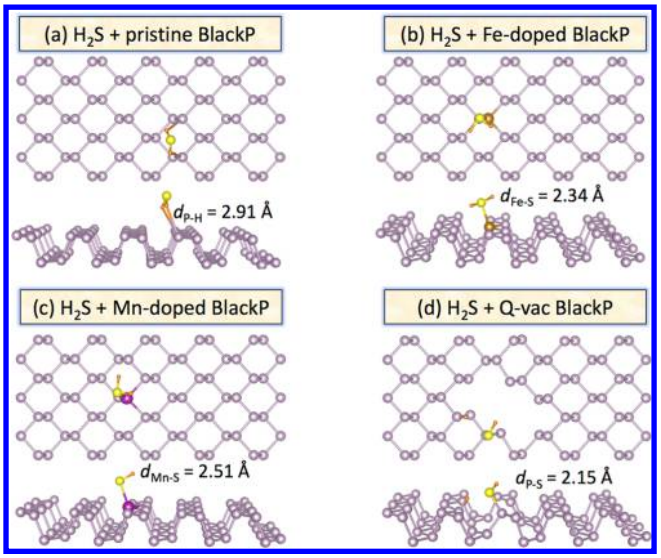

Figure 3. Crystal geometries (bird's-eye and side views) of various types of phosphorene adsorbed by a H_2S molecule: (a) pristine, (b) Fe-doped, (c) Mn-doped, and (d) Quad-vac. Yellow, gold, magenta, and orange balls denote S, Fe, Mn, and H atoms, respectively.

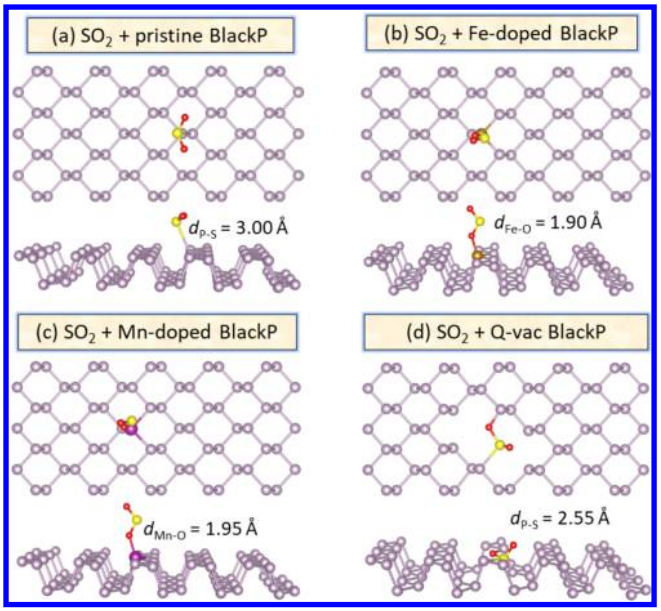

Figure 4. Crystal geometries (bird's-eye and side views) of various types of phosphorene adsorbed by a SO_2 molecule: (a) pristine, (b) Fe-doped, (c) Mn-doped, and (d) Quad-vac. Yellow, gold, magenta, and red balls denote S, Fe, Mn, and O atoms, respectively.

energies. The findings indicate that these gases physisorbed on BlackP via weak vdW forces, resembling the weak adsorption on other elemental 2D materials, namely, graphene nanoribbons,[37] silicene,[38] and germanene.[25] Therefore, the generic elemental 2D materials in pristine forms are chemically insensitive to H_2S and SO_2. The calculated binding energies are much greater than the thermal fluctuation at room temperature (0.03 eV at 300 K). This means that the adsorption of both kinds of gases on the phosphorene surface is a stable process in which the target molecules remain attached to the sensor and the desorption cycles can be done by annealing at the elevated temperature.

In contrast, the presence of impurities can enhance the adsorption energies, particularly for the case of the substitutional doping of Fe and Mn atoms. The adsorption energies of H_2S in Fe(Mn)-doped BlackP are 1.02 (0.81) eV/molecule, around 4 times higher than that in the pristine one. The H_2S molecule is adsorbed on the top site with the horizontal orientation (as shown in Figure 3) where the S atom is located above Fe (Mn) atom to form the Fe (Mn)−S bond with the bond length of 2.34 (2.51) Å, marginally shorter than that in the pristine one. Moreover, the adsorption energies of SO_2 in Fe (Mn)-doped BlackP, as depicted in Figure 4, are 1.01 (0.96) eV/molecule, around 4 times higher than that in pristine. In addition, the adsorption of H_2S onto Fe- and Mn-doped BlackP results in insignificant changes in H−S distances, i.e., 1.364 (1.355) Å in Mn-doped and 1.361 (1.357) in Fe-doped. However, there are increases in the H−S−H bond angle from the original value of 92.1−93.5° in Fe-doped and 92.9° in Mn-doped. Unlike H_2S, the SO_2 molecule energetically favors the top side with the vertical orientation in which one O atom is directed Fe (Mn) atom. The Fe (Mn)−O bond lengths are calculated to be 2.34 (2.51) Å, also remarkably smaller than that of the pristine. The calculated bond lengths between the transition metals and the adsorbed molecules manifest that the chemical bonds are formed because they are in the same order with the combination of metallic radii of transition metals and the covalent radii of S(O) atom. These strong bonds are responsible for the enhanced adsorption energies. Furthermore, the adsorption of SO_2 induces a notable elongation of S−O because of the vertical arrangement of SO_2 where one O atom is directed downward to BlackP. The corresponding S−O distances on Fe- and Mn-doped are 1.462 (1.532) Å and 1.463 (1.539) Å, respectively. Intriguingly, O−S−O bond angles are remarkably bent from the gaseous value of 120.0−113.2° in Fe-doped and 112.9° in Mn-doped.

Regarding the defects, the presence of M-vac and D-vac does not significantly intensify the adsorption energies, meaning that the occurrence of these defects plays an insignificant role in the detection sensitivity of these S-containing gases. Interestingly, Quad-vacant BlackP chemically binds to both kinds of gases with the appropriate adsorption energies. However, the adsorbed molecules get dissociated after adsorption which is not practically suitable for the reversible adsorption−desorption process required for the sensing application.

The gas-binding energies can be qualitatively correlated with the sensitivity by using the statistical thermodynamic model to estimate the adsorption density.[39,40] The interaction between the solid sensor's surface and the adsorbed molecule along z direction can be described by the Morse potential:

$$V(z) = D_e[e^{-2\gamma(z-z_e)} - 2e^{-\gamma(z-z_e)}] \quad (3)$$

where D_e represents the depth of potential well, i.e., binding energy, γ is the fitting parameter, and z_e refers to the equilibrium distance at which the binding energy is at its lowest, as shown in Figure 5. The gas molecule is attached to the sensor when the binding energy becomes negative. Here, the interaction between the gas molecules and the surface's sensor is assumed to be independent in planar $x-y$ plane. This is reasonable because the preferential binding site and orientation was exhaustively searched by sampling various sites and configurations prior to the use of eq 3. The eigenenergies of Schrödinger equation of the adsorbed gas molecule with Morse potential is

DOI: 10.1021/acs.jpcc.8b06803
J. Phys. Chem. C 2018, 122, 20186−20193

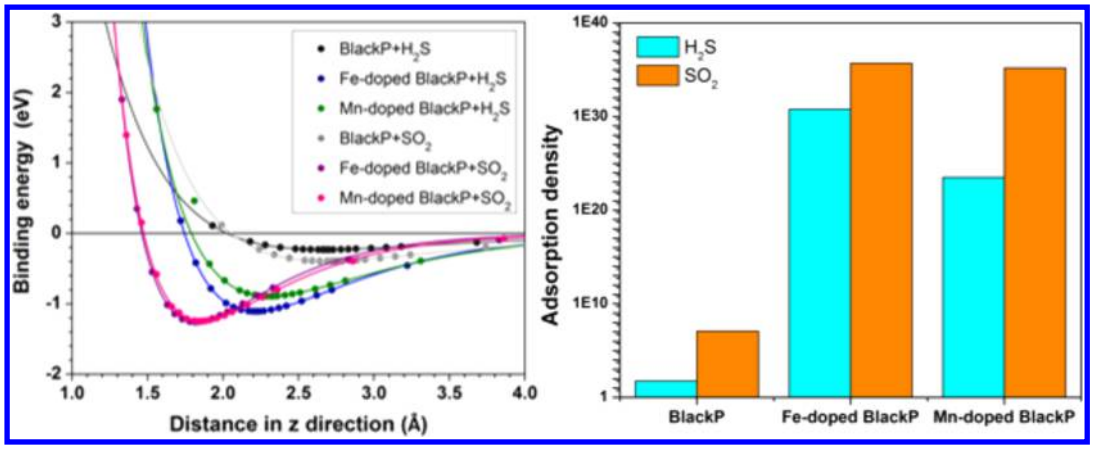

Figure 5. (left) Morse potential as a function of the distance between the BlackP surface and the gas molecule, i.e., the difference in the z coordinate between the top P atom and the closest binding molecule as shown in Figures 3 and 4, and (right) The adsorption densities of H_2S and SO_2 molecules adsorbed on pure and doped BlackP under the gas concentration of 1 ppb at 300 K.

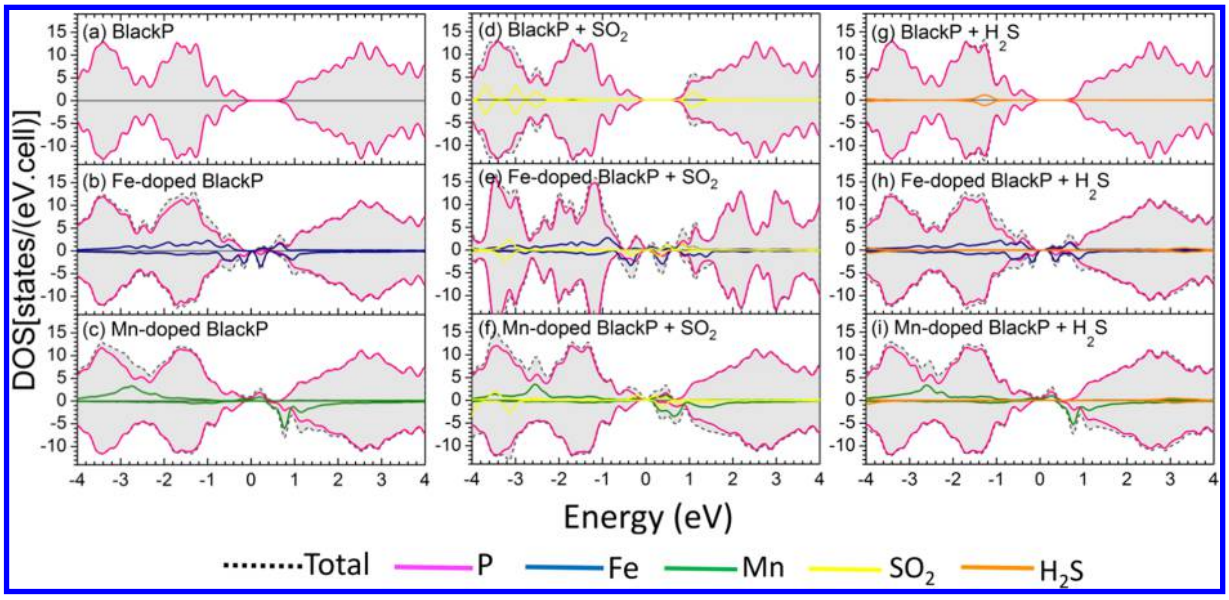

Figure 6. Density of states (DOS) of phosphorene sheets adsorbed by SO_2 and H_2S molecules.

$$E_n = \hbar\omega_g\left[\frac{[-2(2n+1)+8\Delta]^2}{64\Delta}\right] \quad (4)$$

where $\omega_g = \gamma(2D_e/m_g)^2$ defines the characteristic frequency of the gas molecule of mass m_g and $\Delta = D_e/\hbar\omega_g$. The gas adsorption density at the dilute concentration regime, i.e., ignoring the interaction between gas molecules, can be calculated form the number of adsorbed gas molecules (n_g) per unit area (A) according to the expression

$$n_g = \frac{N}{A} = P_g\left[\frac{\lambda}{k_BT}\exp\left(\frac{D_e}{k_BT}\right)\sum_n \exp\left(-\frac{E_n}{k_BT}\right)\right] \quad (5)$$

where the expression in the square bracket is the Henry adsorption isotherm, P_g stands for the partial pressure of the target gas, and we assume it to be 1×10^{-9} which corresponds to the dilute concentration limit. Figure 6 shows the fitting of Morse potential of the gas molecules adsorbed on BlackP and the corresponding adsorption densities under the gas concentration of 1 ppb, i.e., the partial pressure, at 300 K. The densities of H_2S (SO_2) on pristine, Fe-doped, and Mn-doped phosphorene are estimated to be 5.75×10 (1.67×10^7), 5.87×10^{30} (4.96×10^{35}), and 4.26×10^{23} (1.55×10^{35}) cm^{-2}, respectively. It is apparent that the adsorption densities of these S-contained gases on pristine BlackP are remarkably less than those on doped BlackP under the same conditions. This manifests that the latter case offers greater sensitivity to detecting these kinds of gases.

The ultrasensitivities of doped BlackP are comprehensively attributed to the measurable changes in their electronic properties after gas exposure. One can further explore the comprehensive explanations by the analysis of electronic properties via the DOS as depicted in Figure 6. There is no change in the total DOS of pristine BlackP after being adsorbed by H_2S and SO_2. This supports their low adsorption energies and manifests the weak vdW force between BlackP and the adsorbates. The weak vdW-type interaction cannot generate the substantial contrast in the electrical conductivity. It is possible to manipulate the sensitivity by means of surface functionalization by transition metals in order to intensify the charge transfer mechanism. The presence of transition metal (TM) impurities results in the localized 3d-states near the

DOI: 10.1021/acs.jpcc.8b06803
J. Phys. Chem. C 2018, 122, 20186−20193

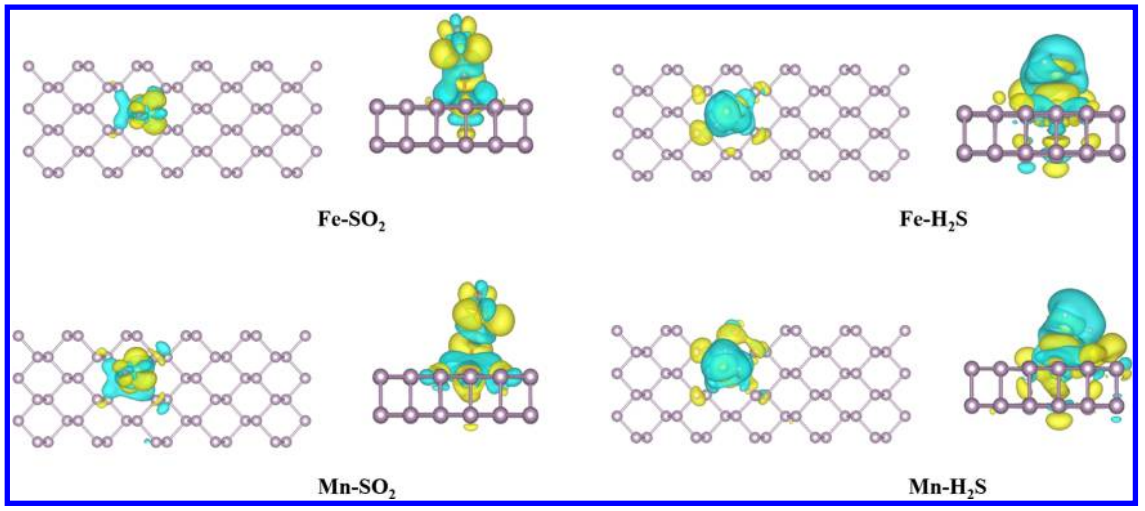

Figure 7. Isosurface charge density of (a) SO_2 + Fe-doped BlackP, (b) H_2S + Fe-doped BlackP, (c) SO_2 + Mn-doped BlackP, and (d) H_2S + Mn-doped BlackP. Yellow and cyan colors represent the accumulation (−) and depletion (+) of electrons, respectively. The charge density is calculated by $n_{gas+BlackP} - (n_{BlackP} + n_{gas})$, where n is charge density. The isosurface presented here is 0.005 e/Å^3.

Fermi level and the systems have become magnetic, see Figure 6b,c, as evident by the calculated magnetic moment of Fe and Mn as 1.40 and 2.80 μ_B, respectively.[41] In principle, the electronic configurations of Fe and Mn are $[Ar]4s^23d^6$ and $[Ar]4s^23d^5$, respectively. Three electrons from the 3d orbitals get involved in forming Fe (Mn)−P bonds with three surrounding phosphorus atoms. This consequently leaves 1 (2) unpaired electrons in the d orbital which are intrinsically prone to incoming gas molecules.

The adsorption of SO_2 creates major changes in the total DOS of the TM doped BlackP, see Figure 6e,f. For the case of SO_2 adsorption on to Fe (Mn)-doped BlackP, there is an intensive overlap between Fe (Mn) 3d and O 2p states to form the strong Fe (Mn)−O ionic bond which is a consequence of the charge transfer from Fe (Mn) 3d to O 2p, i.e., P being highly more electronegative. This transfer mechanism is supported by the graphical plot of charge density shown in Figure 7 where there is charge depletion occurring at the proximity of TM atoms. In contrast, the adsorption of H_2S produces the small changes in DOS of Fe (Mn)-doped, despite the strong adsorption energies previously mentioned. In addition, there are negligible changes in the magnetic moments of Fe (Mn) in Fe (Mn)-doped BlackP after H_2S and SO_2 adsorption. However, these small changes are basically ascribed to the interaction between O 2p orbitals and Fe (Mn) 3d orbitals which leads to spin cancelation. The reduction in magnetic moments is also manifested by the marked change in DOS of Fe (Mn)-doped BlackP after adsorption. This indicates that Fe and Mn impurities do not significantly enhance the sensitivity of BlackP toward H_2S gas. Hence, it is concluded that substitutional doping of Fe to BlackP is a promising approach to enhance the sensitivity of BlackP toward SO_2 detection. Another important parameter that describes the promise of efficient nanosensors is conductivity, which could be calculated by the following relation.

$$\sigma = A \exp(-E_g/2k_BT)$$

where σ is electrical conductivity and E_g, k_B, and T are the band gap, Boltzmann constant and temperature, respectively. A is the constant of proportionality whose value depends on the system.[42] It is apparent from the above relation that the variation of energy gap would directly affect the conductivity of the sensor. Looking at the DOS plots in Figure 6, one can hardly see any change in E_g in the case of pristine phosphorene. However, a careful investigation confirms that both Fe- and Mn-functionalized phosphorene results in an apparent change in E_g upon the exposure of even a single molecule of SO_2. This conductivity change could be converted into an electric signal through an external circuit. Thus, foreign element functionalization enhances the sensing characteristics of phosphorene nanosheets.

CONCLUSION

In summary, we have performed first-principles DFT calculations coupled with the statistical analysis to unravel the structural, electronic, and gas-sensing properties of pristine, defected, and metal-substituted BlackP toward toxic H_2S and SO_2 gas molecules. Our findings have revealed that pristine BlackP weakly interacts with both H_2S and SO_2 by van der Waals (vdW) forces characterized by the small binding energies. The analysis of electronic properties via the DOS indicates that there is a negligible change in DOS after gas exposure which confirms insensitive sensing. To intensity the binding energies, we have considered defects (mono-, di-, tri-, and quad-vacancy) and substitutional impurities (Ti, Si, Mn, and Fe) as the incentives. The presence of mono-and divacancies remains less energetically sensitive to both gas species because of the low adsorption energies. Meanwhile, tri- and quad-vacancies induce the dissociative adsorption, not suitable for the reversible adsorption−desorption cycles. Substitutional doping by Fe atoms is found to be a feasible approach to enhance the sensing resolution of SO_2 detection because of the remarkable adsorption energy incorporated with the substantial variation in DOS after gas exposure. This modification in electronic properties is facilitated by the charge transfer mechanism from Fe 3d to P 3p which can generate the measurable electrical signal detect by the external circuit of the sensor. Our work highlights the functionality of BlackP for detecting toxic SO_2 gas.

DOI: 10.1021/acs.jpcc.8b06803
J. Phys. Chem. C 2018, 122, 20186−20193

AUTHOR INFORMATION

Corresponding Author

*E-mail: tanveer.hussain@uwa.edu.au.

ORCID

T. Kaewmaraya: 0000-0002-0139-1571

A. Karton: 0000-0002-7981-508X

T. Hussain: 0000-0002-0300-0503

Notes

The authors declare no competing financial interest.

ACKNOWLEDGMENTS

T.K. acknowledges the Development and Promotion of Science and Technology Talent Project (DPST) for the financial support of this project (005/2559). The Nanotechnology Centre (NANOTEC), NSTDA Ministry of Science and Technology (Thailand) also supports T.K. through its program of Centre of Excellence Network, Integrated Nanotechnology Research Centre Khon Kaen University (Thailand). In addition, T.K. also acknowledges Prof. Udomsilp Pinsook from the department of Physics, Chulalongkorn University, for providing the kind academic mentoring. We are grateful to Dr Hakkim Vovusha for his useful input in charge density calculations. T.H. and A.K. are indebted to the resources at NCI National Facility systems at the Australian National University through National Computational Merit Allocation Scheme supported by the Australian Government and the University of Queensland Research Computing Centre. A.K. acknowledges an Australian Research Council (ARC) Future Fellowship (FT170100373).

REFERENCES

(1) Umar, A. Sensitivity, Selectivity, and Stability of Gas-Sensitive Metal-Oxide Nanostructures. In *Metal Oxide Nanostructures and Their Applications*; Hahn, Y.-B., Ed.; American Scientific Publishers, 2010.

(2) Schedin, F.; Geim, A. K.; Morozov, S. V.; Hill, E. W.; Blake, P.; Katsnelson, M. I.; Novoselov, K. S. Detection of individual gas molecules adsorbed on graphene. *Nat. Mater.* **2007**, *6*, 652−655.

(3) Kong, J.; Franklin, N. R.; Zhou, C.; Chapline, M. G.; Peng, S.; Cho, K.; Dai, H. Nanotube Molecular Wires as Chemical Sensors. *Science* **2000**, *287*, 622−625.

(4) Comini, E. Metal oxide nanowire chemical sensors: innovation and quality of life. *Mater. Today* **2016**, *19*, 559−567.

(5) Cho, S. Y.; Lee, Y.; Koh, H.-J.; Jung, H.; Kim, J.-S.; Yoo, H.-W.; Kim, J.; Jung, H.-T. Superior Chemical Sensing Performance of Black Phosphorus: Comparison with MoS2 and Graphene. *Adv. Mater.* **2016**, *28*, 7020−8.

(6) Islam, M. S.; Hussain, T.; Rao, G. S.; Panigrahi, P.; Ahuja, R. Augmenting the sensing aptitude of hydrogenated graphene by crafting with defects and dopants. *Sens. Actuators, B* **2016**, *228*, 317−321.

(7) Rao, G. S.; Hussain, T.; Islam, M. S.; Sagynbaeva, M.; Gupta, D.; Panigrahi, P.; Ahuja, R. Adsorption mechanism of graphene-like ZnO monolayer towards CO_2 molecules: enhanced CO_2 capture. *Nanotechnology* **2016**, *27*, 015502−015508.

(8) Perkins, F. K.; Friedman, A. L.; Cobas, E.; Campbell, P. M.; Jernigan, G. G.; Jonker, B. T. Chemical vapor sensing with monolayer MoS2. *Nano Lett.* **2013**, *13*, 668−73.

(9) Kou, L.; Du, A.; Chen, C.; Frauenheim, T. Strain engineering of selective chemical adsorption on monolayer MoS_2. *Nanoscale* **2014**, *6*, 5156−5161.

(10) Li, L.; Yu, Y.; Ye, G. J.; Ge, Q.; Ou, X.; Wu, H.; Feng, D.; Chen, H. X.; Zhang, Y. Black phosphorus field-effect transistors. *Nat. Nanotechnol.* **2014**, *9*, 372−377.

(11) Liu, H.; Neal, A. T.; Zhu, Z.; Luo, Z.; Xu, X.; Tomanek, D.; Ye, P. D. An Unexpected 2D Semiconductor with a high Hole Mobility. *ACS Nano* **2014**, *8*, 4033−4041.

(12) Reich, E. S. Phosphorene Excites Materials Scientists. *Nature* **2014**, *506*, 19.

(13) Radisavljevic, B.; Radenovic, A.; Brivio, J.; Giacometti, V.; Kis, A. Single-layer MoS2 transistors. *Nat. Nanotechnol.* **2011**, *6*, 147−50.

(14) Castellanos-Gomez, A.; Vicarelli, L.; Prada, E.; Island, J. O.; Narasimha-Acharya, K. L.; Blanter, S. I.; Groenendijk, D. J.; Buscema, M.; Steele, G. A.; Alvarez, J. V.; Zandbergen, H. W.; Palacios, J. J.; van der Zant, S. J. Isolation and characterization of few-layer black phosphorus. *2D Mater.* **2014**, *1*, 025001−025019.

(15) Xia, F.; Wang, H.; Jia, Y. Rediscovering black phosphorus as an anisotropic layered material for optoelectronics and electronics. *Nat. Commun.* **2014**, *5*, 4458−4463.

(16) Ray, S. J. First-principles study of MoS2, phosphorene and graphene based single electron transistor for gas sensing applications. *Sens. Actuators, B* **2016**, *222*, 492−498.

(17) Abbas, A. N.; Liu, B.; Chen, L.; Ma, Y.; Cong, S.; Aroonyadet, N.; Kopf, M.; Nilges, T.; Zhou, C. Black Phosphorus Gas Sensor. *ACS Nano* **2015**, *9*, 5618−5624.

(18) Wei, Q.; Peng, X. Superior mechanical flexibility of phosphorene and few-layer black phosphorus. *Appl. Phys. Lett.* **2014**, *104*, 251915−251919.

(19) Mahabal, M.; Deshpande, M. D.; Hussain, T.; Ahuja, R. Sensing Characteristics of Phosphorene Monolayers toward PH_3 and AsH_3 Gases upon the Introduction of Vacancy Defects. *J. Phys. Chem. C* **2016**, *120*, 20428−20436.

(20) Lee, G.; Kim, S.; Jung, S.; Jang, S.; Kim, J. Suspended black phosphorus nanosheet gas sensors. *Sens. Actuators, B* **2017**, *250*, 569−573.

(21) Cui, S.; Pu, H.; Wells, S. A.; Wen, Z.; Mao, S.; Chang, J.; Hersam, M. C.; Chen, J. Ultrahigh sensitivity and layer-dependent sensing performance of phosphorene-based gas sensors. *Nat. Commun.* **2015**, *6*, 8632−8640.

(22) Yang, Q.; Meng, R.-S.; Jiang, J.-K.; Liang, Q.-H.; Tan, C.-J.; Cai, M.; Sun, X.; Yang, D.-G.; Ren, T.-L.; Chen, X.-P. First-Principles Study of Sulfur Dioxide Sensor Based on Phosphorenes. *IEEE Electron Device Lett.* **2016**, *37*, 660−662.

(23) Cho, S.-Y.; Kim, S. J.; Lee, Y.; Kim, J.-S.; Jung, W.-B.; Yoo, H.-W.; Kim, J.; Jung, H.-T. Highly Enhanced Gas Adsorption Properties in Vertically Aligned MoS2 Layers. *ACS Nano* **2015**, *9*, 9314−21.

(24) Sarkar, D.; Xie, X.; Kang, J.; Zhang, H.; Liu, W.; Navarrete, J.; Moskovits, M.; Banerjee, K. Functionalization of transition metal dichalcogenides with metallic nanoparticles: implications for doping and gas-sensing. *Nano Lett.* **2015**, *15*, 2852−2862.

(25) Hussain, T.; Kaewmaraya, T.; Chakraborty, S.; Vovusha, H.; Amornkitbamrung, V.; Ahuja, R. Defected and Functionalized Germanene-based Nanosensors under Sulfur Comprising Gas Exposure. *ACS Sensors* **2018**, *3*, 867−874.

(26) Kresse, G.; Furthmüller, J. Efficient iterative schemes for ab initio total-energy calculations using a plane-wave basis set. *Phys. Rev. B: Condens. Matter Mater. Phys.* **1996**, *54*, 11169−11186.

(27) Blochl, P. E. Projector augmented-wave method. *Phys. Rev. B: Condens. Matter Mater. Phys.* **1994**, *50*, 17953−17979.

(28) Perdew, J. P.; Burke, K.; Ernzerhof, M. Generalized Gradient Approximation Made Simple. *Phys. Rev. Lett.* **1996**, *77*, 3865−3868.

(29) Grimme, S. Semiempirical GGA-type density functional constructed with a long-range dispersion correction. *J. Comput. Chem.* **2006**, *27*, 1787−99.

(30) Yu, M.; Trinkle, D. R. Accurate and efficient algorithm for Bader charge integration. *J. Chem. Phys.* **2011**, *134*, 064111−064118.

(31) Qiao, J.; Kong, X.; Hu, Z.-X.; Yang, F.; Ji, W. High-mobility transport anisotropy and linear dichroism in few-layer black phosphorus. *Nat. Commun.* **2014**, *5*, 4475−4481.

(32) Li, X.-B.; Guo, P.; Cao, T.-F.; Liu, H.; Lau, W.-M.; Liu, L.-M. Structures, stabilities, and electronic properties of defects in monolayer black phosphorus. *Sci. Rep.* **2015**, *5*, 10848−10858.

DOI: 10.1021/acs.jpcc.8b06803
J. Phys. Chem. C 2018, 122, 20186−20193

(33) Banhart, F.; Kotakoski, J.; Krasheninnikov, V. Structural Defects in graphene. *ACS Nano* **2011**, *5*, 26−41.
(34) Huang, B.; Li, Z.; Liu, Z.; Zhou, G.; Hao, S.; Wu, J.; Gu, B.-L.; Duan, W. Adsorption of Gas Molecules on Graphene Nanoribbons and Its Implication for Nanoscale Molecule Sensor. *J. Phys. Chem. C* **2008**, *112*, 13442−13446.
(35) Hussain, T.; Hankel, M.; Searles, D. J. Improving Sensing of Sulfur-Containing Gas Molecules with ZnO Monolayers by Implanting Dopants and Defects. *J. Phys. Chem. C* **2017**, *121*, 24365−24375.
(36) Abdulkader Tawfik, S.; Cui, X. Y.; Carter, D. J.; Ringer, S. P.; Stampfl, C. Sensing sulfur-containing gases using titanium and tin decorated zigzag graphene nanoribbons from first-principles. *Phys. Chem. Chem. Phys.* **2015**, *17*, 6925−6932.
(37) Shao, L.; Chen, G.; Ye, H.; Niu, H.; Wu, Y.; Zhu, Y.; Ding, B. Sulfur dioxide molecule sensors based on zigzag graphene nanoribbons with and without Cr dopant. *Phys. Lett. A* **2014**, *378*, 667−671.
(38) Hussain, T.; Kaewmaraya, T.; Chakraborty, S.; Ahuja, R. Defect and Substitution-Induced Silicene Sensor to Probe Toxic Gases. *J. Phys. Chem. C* **2016**, *120*, 25256−25262.
(39) Pu, H. H.; Rhim, S. H.; Gajdardziksa-Josifovska, M.; Hirschmugl, C. J.; Weinert, M.; Chen, J. H. A statistical thermodynamics model for monolayer gas adsorption on graphene-based materials: implications for gas sensing applications. *RSC Adv.* **2014**, *4*, 47481−47487.
(40) Li, P.; Zhang, D.; Jiang, C.; Zong, X.; Cao, Y. Ultra-sensitive suspended atomically thin-layered black phosphorus mercury sensors. *Biosens. Bioelectron.* **2017**, *98*, 68−75.
(41) Hashmi, A.; Hong, J. Transition Metal Doped Phosphorene: First-Principles Study. *J. Phys. Chem. C* **2015**, *119*, 9198−9204.
(42) Nagarajan, V.; Chandiramouli, R. Sensing properties of monolayer borophene nanosheet towards alcohol vapors: a first-principles study. *J. Mol. Graphics Modell.* **2017**, *73*, 208−216.

DOI: 10.1021/acs.jpcc.8b06803
J. Phys. Chem. C 2018, 122, 20186−20193